# UCLA

## UCLA Previously Published Works

**Title**

Bruchi¯s membrane opening-minimum rim width and visual field loss in glaucoma: a broken stick analysis

**Permalink**

**Journal**

**ISSN**

**Authors**

Park, Keun-Heung
Lee, Ji-Woong
Kim, Jin-Mi
et al.

**Publication Date**

**DOI**

Peer reviewed

• Clinical Research •

# Bruch's membrane opening-minimum rim width and visual field loss in glaucoma: a broken stick analysis

*Keun-Heung Park[1], Ji-Woong Lee[1,2], Jin-Mi Kim[3], Kouros Nouri-Mahdavi[4], Joseph Caprioli[4]*

[1]Department of Ophthalmology, Pusan National University College of Medicine, Busan 49241, Korea
[2]Biomedical Research Institute, Pusan National University Hospital, Busan 49241, Korea
[3]Department of Biostatistics, Clinical Trial Center, Biomedical Research Institute, Pusan National University Hospital, Busan 49241, Korea
[4]Stein Eye Institute, David Geffen School of Medicine at UCLA, Los Angeles 90095, California, USA
**Correspondence to:** Ji-Woong Lee. Department of Ophthalmology, Pusan National University College of Medicine, 179 Gudeok-ro, Seo-gu, Busan 49241, Korea. glaucoma@pnu.ac.kr
Received: 2017-04-05        Accepted: 2017-12-05

## Abstract

● **AIM:** To determine the Bruch's membrane opening-minimum rim width (BMO-MRW) tipping point where corresponding visual field (VF) damages become detectable.

● **METHODS: A total of 85 normal subjects and 83 glaucoma patients (one eye per participant) were recruited for the study. All of the patients had VF examinations and spectral-domain optical coherence tomography to measure the BMO-MRW. Total deviation values for 52 VF points were allocated to the corresponding sector according to the Garway-Heath distribution map. To evaluate the relationship between VF loss and BMO-MRW measurements, a "broken-stick" statistical model was used. The tipping point where the VF values started to sharply decrease as a function of BMO-MRW measurements was estimated and the slopes above and below this tipping point were compared.**

● **RESULTS: A 25.9% global BMO-MRW loss from normative value was required for the VF loss to be detectable. Sectorally, substantial BMO-MRW thinning in inferotemporal sector (33.1%) and relatively less BMO-MRW thinning in the superotemporal sector (8.9%) were necessary for the detection of the VF loss. Beyond the tipping point, the slopes were close to zero throughout all of the sectors and the VF loss was unrelated to the BMO-MRW loss. The VF loss was related to the BMO-MRW loss below the tipping point. The difference between the two slopes was statistically significant (*P*≤0.002).**

● **CONCLUSION: Substantial BMO-MRW loss appears to be necessary for VF loss to be detectable in patients with open angle glaucoma with standard achromatic perimetry.**

● **KEYWORDS:** Bruch's membrane opening-minimum rim width; visual field loss; structure function relationship; broken stick model; optical coherence tomography

## INTRODUCTION

Glaucoma is a chronic optic neuropathy characterized by the progressive decrease of retinal ganglion cells (RGCs) and their axons, resulting in thinning of the neuroretinal rim of the optic nerve head (ONH) and retinal nerve fiber layer (RNFL), and eventually leading to visual field (VF) defects[1].

The diagnosis of glaucoma and the detection of progression are based on a combination of structural and functional tests[2-3]. However, discordance between structural and functional testing should be expected in patients with glaucoma[4-5]. Optic disc damage and RNFL defects may precede the beginning of glaucomatous VF loss[6-7]. Kerrigan-Baumrind *et al*[8] reported that a 25%-35% RGC loss was associated with statistical abnormalities in automated VF testing. Other studies have reported that a 8%-42% RNFL loss, as measured using spectral-domain optical coherence tomography (SD-OCT), was required for functional loss to be detectable[9-10]. Most importantly, detection of early structural changes that can precede VF loss is fundamental to the long-term preservation of vision in glaucoma patients[6-10].

The SD-OCT enabled clinicians to characterize the ONH anatomy in relation to the clinical optic disc margin[11]. Recently, Reis *et al*[12] introduced a new anatomical parameter of neuroretinal rim, Bruch's membrane opening-minimum rim width (BMO-MRW), which quantifies the neuroretinal rim from BMO's inner end and accounts for the variable trajectory of RGC axons at the measurement points. This parameter consists of the shortest distance between the BMO and the internal limiting membrane (ILM), and has been reported to

yield better diagnostic accuracy and more accurate structure-function relationship than the disc margin-based rim area[13-16]. However, none of these studies identified the threshold value of the BMO-MRW at which the functional loss as measured with standard automated perimetry can be detected. Therefore, the purpose of this study was to determine the BMO-MRW tipping point at which the VF loss was detectable and related to structural changes.

**SUBJECTS AND METHODS**

**Participants**  In this retrospective, cross-sectional study, open angle glaucoma patients and normal subjects who were seen at the Glaucoma Clinic at Pusan National University Hospital between August 1, 2015 and January 31, 2016 were included. The study was conformed to the tenets of the Declaration of Helsinki and was approved by the Institutional Review Board (IRB) of Pusan National University Hospital. The written consent from patients was waived by IRB because this is a retrospective, anonymous study. When both eyes of a participant were eligible, one eye was randomly chosen for inclusion in the study.

All of the enrolled glaucoma patients and healthy subjects underwent a complete ophthalmic examination, including measurement of the best-corrected visual acuity (BCVA), a slit-lamp examination, gonioscopy, funduscopy, biometry using an IOL Master (Carl Zeiss Meditec, Dublin, CA, USA), and standard automated perimetry. Central corneal thickness was measured using ultrasonic pachymetry (Pachmate; DGH Technology, Exton, PA, USA). Keratometry and spherical equivalent were measured with an Auto Kerato-Refractometer (ARK-510A; NIDEK, Hiroishi, Japan). All of the patients were also examined using red-free RNFL photographs, optic disc stereoscopic photographs, and SD-OCT images (Spectralis; Heidelberg Engineering, Heidelberg, Germany). The inclusion criteria for the participants included an age >18y with a clear cornea and clear ocular media, a BCVA≥20/40, a refractive error within ±6.0 diopters (D) of 0, and astigmatism ±3.0 D of 0. Exclusion criteria included diabetes, uveitis, secondary glaucoma, corneal abnormalities, non-glaucomatous optic neuropathies, previous trauma, ocular surgery or laser treatment, or any other eye disease other than glaucoma. Eyes were classified as having open angle glaucoma if they had a glaucomatous optic disc and two consecutive abnormal VF test results with open angles on gonioscopy. Glaucomatous optic neuropathy was defined as having a >0.2 cup-to-disc ratio asymmetry between the two eyes, neuroretinal rim thinning, notching, or characteristic RNFL defects indicative of glaucoma[17]. Healthy subjects were recruited among those who visited this hospital for regular health check-ups or refractive errors. They were defined as those with no history of ocular disease, an intraocular pressure <21 mm Hg, an absence of glaucomatous optic disc appearance, and a normal VF. Subjects who were clinically suspected to have glaucoma because of
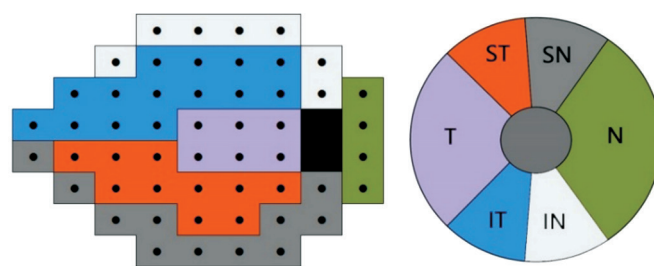


**Figure 1 Garway-Heath sectorization of Bruch's membrane opening-minimum rim width and corresponding VF threshold values** ST: Superotemporal sector; T: Temporal sector; IT: Inferotemporal sector; IN: Inferonasal sector; N: Nasal sector; SN: Superonasal sector.

ONH or RNFL appearance, or elevated intraocular pressure but with normal VF were included in the healthy subjects to ensure representation of the full spectrum of disease.

**Perimetric Tests**  All VF tests were performed with an automated VF analyzer (Humphrey Field Analyzer; Carl Zeiss Meditec, Inc., Dublin, CA, USA) with a 24-2 pattern and a size III white stimulus using the Swedish Interactive Threshold Algorithm (SITA) standard strategy. Reliable tests were defined as <20% fixation loss rate, <15% false-positive rate, and <33% false-negative rate.

Normal subjects had a Glaucoma Hemifield Test (GHT) within normal limits and a mean deviation (MD) and pattern standard deviation (PSD) within 95% of HFA's normative database. An abnormal VF was defined as $P<0.05$ for the PSD or a GHT result outside of the normal limits. The total deviation (TD) values were recorded in all of the 52 testing points (points matching the blind spot were excluded) and then assigned to the corresponding VF sector according to the Garway-Heath distribution map[18]. The TD values in dB unit was first converted to linear (1/Lambert) scale with the following formula; $1/\text{Lambert} =10^{dB/10}$, then averaged in each sector, and converted back to the decibel scale for analysis[19] (Figure 1).

**Spectral-domain Optical Coherence Tomography Imaging** SD-OCT was performed on all of the subjects on the same day as the perimetric test. Scans were acquired according to the participant's specific fovea-BMO axis to minimize the geometrical errors[15], and the data were sectorized according to this axis. The fovea position was manually located with a live B-scan, followed by the two BMO points in each of two radial B-scans that were perpendicular to each other. A radial pattern containing 24 angular, equidistant, high-resolution 15° B-scans centered on the BMO was used to compute the neuroretinal rim parameters. Each B-scan was averaged from 25 individual scans with 1536 A-scans per B-scan with a scanning speed of 40 000 A-scans per second[10,20]. The BMO points and ILM were identified and marked in each B-scan with automated software (Glaucoma Module Premium Edition, version 6.0; Heidelberg Engineering) and corrected when necessary. Eyes with an image quality score <20 were excluded. BMO-MRW,

the minimum distance between the BMO and ILM, was automatically computed globally and sectorally according to the Garway-Heath distribution map corresponding to the VF sectors[18]. The Spectralis OCT used TruTrack™ that used dual beam technology to compensation for eye motion[10,20]. One beam captured an image of the retina and mapped over 1000 points to track eye movement. With this map as a reference, the second beam was directed to the desired location despite of eye movements.

**Statistical Analysis** The normality of the data distribution was checked using the Kolmogorov-Smirnov test. Clinical characteristics of the study population were compared using Student's *t*-test or the Mann-Whitney *U* test for continuous variables, and the $\chi^2$ test for categorical variables.

A scatterplot of the BMO-MRWs with the VF TD values showed a plateau of the VF at high BMO-MRW values and a steep decrease at lower BMO-MRW values. A nonlinear "broken stick" statistical model was used to fit this scatter plot. An initial estimate of the tipping point was determined using Davies' test[21], after which segment regression analyses were performed with this initial tipping point as a starting value. Using iteration of segment regression analyses to reduce error, the final tipping point and two slopes of the broken stick model with their corresponding 95% confidence intervals (CIs) were determined. All of the statistical analyses were performed using R language software (http://www.R-project.org) and the segmented R library[22]. A value of *P*<0.05 was considered statistically significant.

## RESULTS

One hundred sixty-eight participants (85 normal and 83 glaucoma subjects) were enrolled in the study. The demographic, clinical, and ocular characteristics of the participants are summarized in Table 1. The global BMO-MRW of the glaucoma patients was significantly thinner than that of the normal subjects, 256.3±48.9 μm for the normal subjects and 163.8±37.9 μm for the glaucoma patients (*P*<0.001). The number of glaucoma patients whose sectoral BMO-MRW values followed the ISNT rule was significantly lower than the normal subjects, with 31 (36.5%) for the normal subjects and 3 (3.6%) for the glaucoma patients (*P*<0.001; Table 2). The global indices of the VF for glaucoma patients were significantly worse than the normal subjects. The VF MD was -1.22±1.91 dB for the normal subjects and -7.06±5.38 dB for glaucoma patients (*P*<0.001).

Scatterplots of the global, sectoral BMO-MRWs and corresponding VF TD values are shown in Figures 2 and 3. A range of BMO-MRW values was unrelated to the VF TD values, followed by a range of BMO-MRW values which was strongly related to the VF TD values (Figure 2A). Statistically optimal locations of the tipping points between these two ranges in the global and sectoral BMO-MRW values are summarized in Table 3. The locations of the tipping

**Table 1 Demographic and clinical characteristics of the study groups based on the diagnosis in 168 eyes of 168 subjects**

| Items | Healthy (*n*=85) | Glaucoma (*n*=83) | *P* |
|---|---|---|---|
| Age (y) | 56.6±12.9 | 59.4±13.8 | 0.106[a] |
| Female/male | 43/42 | 39/44 | 0.647[b] |
| Axial length (mm) | 23.71±1.17 | 24.09±1.46 | 0.081[c] |
| Central corneal thickness (μm) | 552.4±39.0 | 543.3±37.4 | 0.132[c] |
| Spherical equivalent (D) | -0.94±2.37 | -1.25±2.62 | 0.445[a] |
| Intraocular pressure (mm Hg) | 14.4±3.2 | 15.5±4.3 | 0.078[a] |
| VF | | | |
| Mean deviation (dB) | -1.22±1.91 | -7.06±5.38 | <0.001[a] |
| Pattern standard deviation (dB) | 1.90±1.38 | 6.77±4.15 | <0.001[a] |
| VFI (%) | 98.49±2.64 | 81.71±16.77 | <0.001[a] |

[a]Mann-Whitney *U* test; [b]$\chi^2$ test; [c]Student's *t*-test. VF: Visual field; VFI: Visual field index.

**Table 2 BMO-MRW values and the percentage of healthy and glaucoma subjects that met the ISNT rule for BMO-MRW**

μm; mean±SD

| BMO-MRW area | Healthy (*n*=85) | Glaucoma (*n*=83) | *P* |
|---|---|---|---|
| Global | 256.3±48.9 | 163.8±37.9 | <0.001[b] |
| Superotemporal | 254.0±56.8 | 160.4±53.8 | <0.001[b] |
| Temporal | 185.1±42.6 | 131.6±41.2 | <0.001[b] |
| Inferotemporal | 283.1±51.3 | 140.8±63.3 | <0.001[a] |
| Superonasal | 297.1±66.7 | 191.1±57.6 | <0.001[b] |
| Nasal | 272.0±64.0 | 184.4±46.9 | <0.001[a] |
| Inferonasal | 307.7±59.3 | 178.3±57.1 | <0.001[b] |
| ISNT rule met[d] | 31 (36.5%) | 3 (3.6%) | <0.001[c] |

[a]Mann-Whitney *U* test; [b]Student's *t*-test; [c]$\chi^2$ test; [d]The number of patients whose BMO-MRW values met the ISNT rule. The ISNT rule was met when the BMO-MRW was thickest based on the average of the two inferior quadrants, followed by the average of the two superior, nasal, and then temporal quadrants. BMO-MRW: Bruch's membrane opening-minimum rim width.

points were statistically significant for all of the locations (all *P*≤0.006; Davies' test). The percentages of BMO-MRW loss for the tipping points were calculated for the global and sectoral BMO-MRW values using the mean BMO-MRW values for the normal subjects. The tipping point for the global BMO-MRW measurement occurred after a 25.9% loss from the mean normal BMO-MRW value. Using sectoral analyses, the percentage of BMO-MRW loss was highest for the superonasal sector (34.9%) and was lowest loss for the temporal sector (6.6%), with a range of 8.9%-34.4% for all of the other sectors (Table 3).

The slopes for VF TD values as a function of BMO-MRWs above and below the tipping points and the differences between the slopes are summarized in Table 4. Above the tipping points, the slopes of the VF TD values to BMO-MRW values were not different from zero (*i.e.* the 95%CIs included zero) throughout
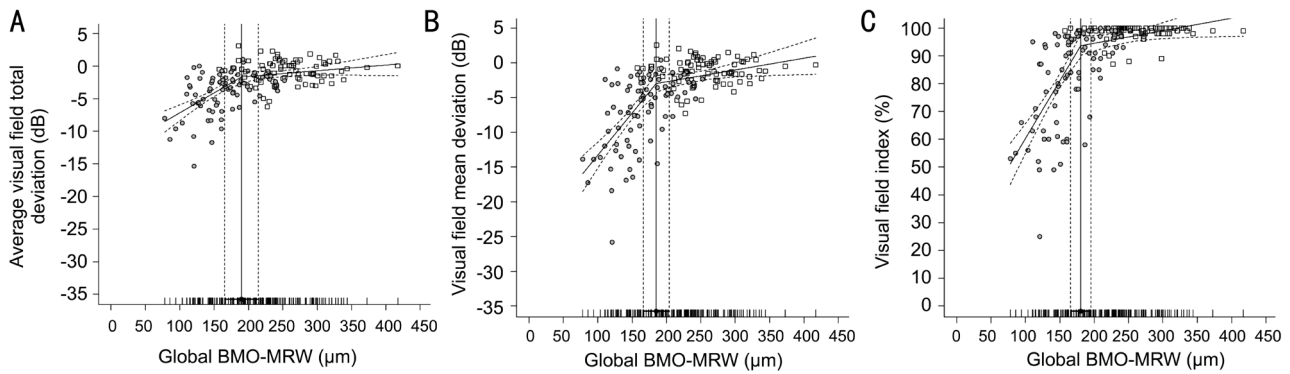
**Figure 2 Scatter plots of the global mean BMO-MRW with the corresponding VF total deviation values (A), mean deviation (B) and VFI (C) in healthy (empty squares) and glaucoma (filled circles) eyes** The 95%CIs for the tipping points and slopes are shown as dashed line. The tipping points are 189.8 μm (A), 185.0 μm (B) and 180.4 μm (C).
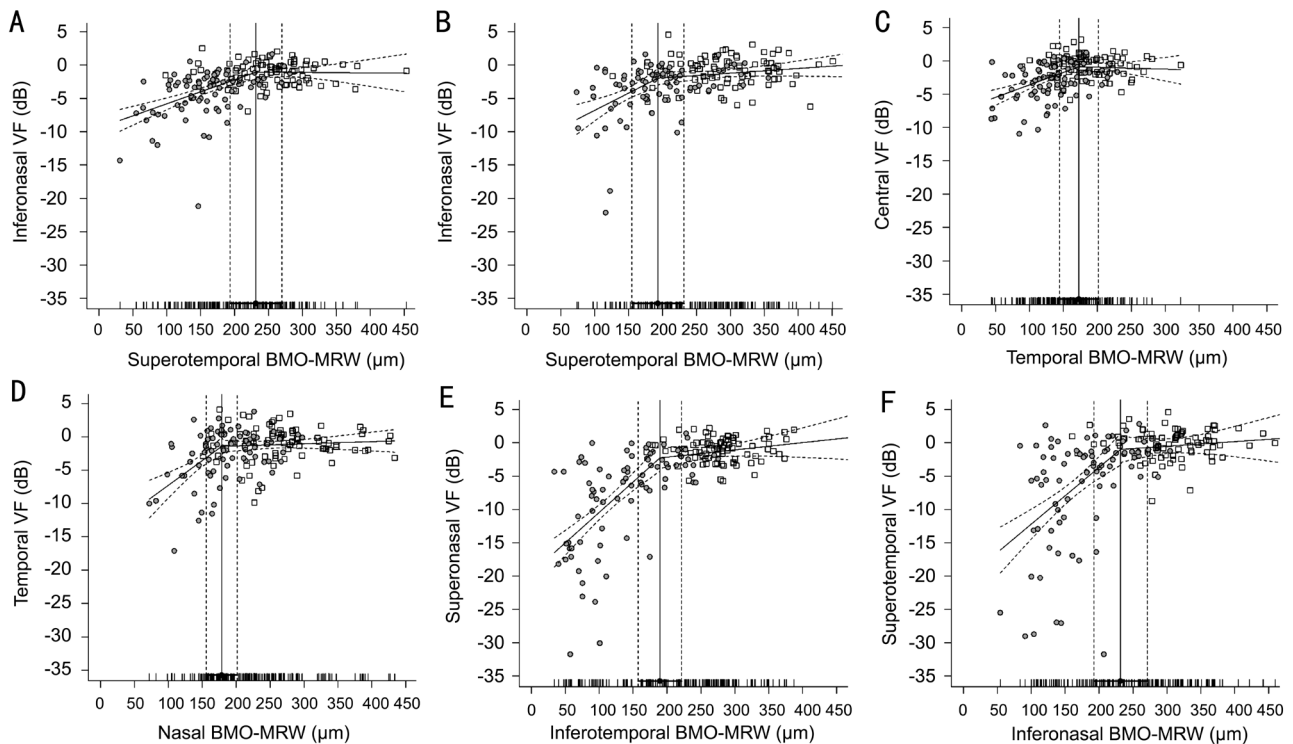


**Figure 3 Scatter plots of healthy (empty squares) and glaucoma (filled circles) BMO-MRW in each sector with corresponding VF threshold values** The 95%CIs for the tipping point and slopes are shown as dashed line.

**Table 3 The global and sectoral BMO-MRW tipping points with percent loss from the average normal values**

| BMO-MRW area | BMO-MRW tipping point (95%CI) | [a]Loss tipping point from normative (%) | [b]P |
|---|---|---|---|
| Global | 189.8 (165.2 to 214.4) | 25.9 | <0.001 |
| Superotemporal | 231.5 (193.1 to 269.8) | 8.9 | 0.003 |
| Temporal | 172.9 (144.4 to 201.5) | 6.6 | 0.006 |
| Inferotemporal | 189.3 (157.3 to 221.3) | 33.1 | <0.001 |
| Superonasal | 193.3 (154.7 to 231.8) | 34.9 | 0.006 |
| Nasal | 178.4 (155.1 to 201.7) | 34.4 | <0.001 |
| Inferonasal | 231.7 (192.2 to 271.2) | 24.7 | <0.001 |

[a]Average percent BMO-MRW thickness loss associated with each tipping point value. The normative values are from current study healthy group; [b]P value from Davies' test which means the tipping point is statistically significant. BMO-MRW: Bruch's membrane opening-minimum rim width.

all of the sectors and global BMO-MRW. However, the slopes below the tipping point were significantly different from zero throughout the all of the sectors and global BMO-MRW (all $P<0.001$). In addition, the slopes below the tipping point were significantly steeper than the slopes above the tipping point (superonasal sector, $P=0.002$; all other sectors, $P<0.001$).

Globally, the tipping point was estimated at 189.8 μm (95%CI, 165.2 to 214.4), with a slope above the tipping point of 0.009 dB/μm (95%CI, -0.002 to 0.019) and below the tipping point of 0.061 dB/μm (95%CI, 0.040 to 0.082). Using the same approach with the VF MD instead of the TD values, the tipping point was 185.0 μm (95%CI, 166.3 to 203.8) with a slope above the tipping point of 0.017 dB/μm (95%CI, 0.002 to 0.032) and below the tipping point of 0.121 dB/μm (95%CI, 0.087 to 0.156), with a statistically significant difference

**Table 4 Slopes associated with the broken stick model used to determine the tipping point (point at which BMO-MRW thinning is first associated with VF loss)**

| BMO-MRW area | Slopes below the tipping point (dB/μm) | | | Slopes above the tipping point (dB/μm) | | | Difference between the slopes | | | Adjusted $R^2$ |
|---|---|---|---|---|---|---|---|---|---|---|
| | Slope | 95%CI | [a]P | Slope | 95%CI | [a]P | △ Slope | 95%CI | [b]P | |
| Global | 0.061 | 0.040 to 0.082 | <0.001 | 0.009 | -0.002 to 0.019 | 0.101 | -0.052 | -0.084 to -0.021 | <0.001 | 0.3645 |
| Superotemporal | 0.036 | 0.024 to 0.048 | <0.001 | 0.000 | -0.017 to 0.016 | 0.951 | -0.036 | -0.065 to -0.008 | <0.001 | 0.2929 |
| Temporal | 0.037 | 0.023 to 0.052 | <0.001 | -0.003 | -0.021 to 0.015 | 0.748 | -0.040 | -0.073 to -0.008 | <0.001 | 0.2027 |
| Inferotemporal | 0.091 | 0.068 to 0.115 | <0.001 | 0.011 | -0.005 to 0.027 | 0.191 | -0.081 | -0.120 to -0.041 | <0.001 | 0.5264 |
| Superonasal | 0.052 | 0.025 to 0.078 | <0.001 | 0.007 | -0.002 to 0.016 | 0.115 | -0.045 | -0.080 to -0.009 | 0.002 | 0.2136 |
| Nasal | 0.074 | 0.039 to 0.110 | <0.001 | 0.003 | -0.006 to 0.012 | 0.477 | -0.071 | -0.116 to -0.027 | <0.001 | 0.1800 |
| Inferonasal | 0.085 | 0.056 to 0.115 | <0.001 | 0.007 | -0.015 to 0.028 | 0.530 | -0.078 | -0.130 to -0.028 | <0.001 | 0.3425 |

[a]P values for the slopes below and above the tipping point represent the statistical significance of the slopes being different than zero; [b]P values represent the statistical significance of the difference between the slopes below and above the tipping points. Values of fitted slopes below and above the tipping point are listed for global and quadrant BMO-MRW. BMO-MRW: Bruch's membrane opening-minimum rim width.

between the slopes ($P<0.001$; Figure 2B). A similar segmented structure-function relationship was found using the visual field index (VFI). The tipping point was 180.4 μm (95%CI, 165.7 to 195.0) with a slope above the tipping point of 0.045 dB/μm (95%CI, 0.004 to 0.087) and below the tipping point of 0.415 dB/μm (95%CI, 0.314 to 0.516), with a statistically significant difference between the slopes ($P<0.001$; Figure 2C).

## DISCUSSION

We determined the relationship between the BMO-MRW and VF sensitivity using the broken stick tipping point model. We identified the tipping point where the VF abnormality was associated with the BMO-MRW loss. Overall, the result showed that a substantial BMO-MRW loss (25.9% loss from the average normal global value) was necessary to detect the VF loss.

Determination of the actual location of the expected VF loss is clinically important in preserving vision in patients with suspected or preperimetric glaucoma[9-10,23]. We also found that substantial BMO-MRW thinning in inferotemporal sector (33.1%) and relatively less BMO-MRW thinning in the superotemporal sector (8.9%) were necessary for the detection of the VF loss. In the temporal sector, only 6.6% of the BMO-MRW loss was necessary for the detection of the VF loss.

The results in this study were consistent with the earlier studies, which reported that substantial structural loss was necessary before functional VF defects became detectable[6-10]. Wollstein et al[9] reported that a loss >17.3% of the mean RNFL thickness was necessary for the VF defect to be detectable. The authors reported that losses of 27.8% and 25.8% of RNFL thickness in the superior and inferior quadrants, respectively, were necessary before the VF defect was detectable[9]. Alasil et al[10] demonstrated that detectable VF defects were associated with 42.3% and 14.5% thinning of the RNFL thickness in the inferior and superior quadrants, respectively. They also found that the temporal quadrant showed the lowest

percentage RNFL loss needed to detect the central VF loss[9-10]. The normal neural rim width is thickest in the inferior region, followed by the superior, nasal and temporal regions (ISNT rule)[24]. We showed that the BMO-MRW values also followed the ISNT rule in normal subjects. It can therefore be inferred that sectors with the thicker BMO-MRW may require more structural loss for corresponding functional abnormality to be detectable[9-10]. The number of axons passing through the temporal region of the optic disc was significantly larger than other regions because of the high concentration of thinner axons in the papillomacular bundle[9,25]. Based on our study, this might lead to the development of VF damage after a smaller BMO-MRW loss.

In this study, the regression slopes of VF TD values to the BMO-MRW above the tipping points were not different from zero in all of the locations. These results are consistent with clinical experience and findings in the literature, suggesting that many patients may show evidence of ONH damage before functional loss such as VF is detected[7,26-27]. Similarly, there was a poor association of the RNFL thickness with the VF loss when the loss of RNFL thickness was not severe[9-10,28-30]. Yu et al[31] found that progressive RNFL thinning strongly predicted a subsequent VF decline.

We showed that the slopes of the VF TD values to the BMO-MRW below the tipping point were significantly steeper than the slopes above the tipping point for all of the locations. It is possible that a strong clinical relationship between structure and function may be detected only after the redundancy of RGC function was exhausted[32]. The reasons for the discordance in structure-function relationship in our study were likely because standard automated perimetry had higher variability than OCT during the early development of glaucoma[19,33]. Because of the redundancy of VF sensitivity, damage occurred without showing early abnormalities[32-33]. In addition, global indices of the VF such as MD and VFI are insensitive to localized loss[34] and less able to detect early glaucoma because of the

ceiling effect[35]. Gardiner et al[36] reported that both structural and functional tests were associated with significant intra-individual and inter-test variability, and the weak structure-function relationship in ocular hypertension or suspected/early glaucoma could be explained by variability in testing. Subtle rotation of eye and head tilt can skew the OCT measurement, and each sectoral mean may differ without any actual changes in the ONH[37]. However, Spectralis OCT uses TruTrack™ that uses dual beam technology to compensate for possible eye motion to reduce the measurement variability[10,20]. Taken together, the results suggested that a combination of structural and functional assessment are very important in the evaluation of the early glaucomatous damage and disease progression in patients with glaucoma[10,14,33].

Recently, an anatomically and geometrically accurate rim parameter based on the BMO was reported[12-13,15]. This new parameter, termed the BMO-MRW, quantifies the neuroretinal rim from the actual anatomical outer border and accounts for the variable orientation of the rim tissue in ONH[12-13,15]. The BMO-MRW has better diagnostic accuracy[13] and a stronger relationship to the VF than the RNFL thickness and other neuroretinal rim measurement[14-15]. Chauhan et al[13] reported that at 95% specificity, the sensitivity of the RNFL thickness, BMO-HRW, and BMO-MRW was 70%, 51%, and 81%, respectively. Pollet-Villard et al[14] reported that the structure-function relationship with the BMO-MRW was stronger than that with either the RNFL thickness or the Cirrus high definition OCT based neuroretinal rim measures. Danthurebandara et al[15] reported that the structure-function relationship was stronger with the BMO-MRW than with the disc margin-based rim area and the BMO based horizontal rim width (BMO-HRW). Our study differed from previous studies that used a single linear or logarithmic regression model to evaluate structure-function relationship with the BMO-MRW[14-15]. In contrast to these previous studies, our study used the broken stick tipping point model to show that the BMO-MRW had a strong association with VF loss. We also performed analyses using the MD and VFI since they are commonly used functional parameters in clinical practice. The tipping points for MD and VFI occured at a BMO-MRW value of 185.0 µm and 180.4 µm, respectively.

A proportion of neuroretinal rim area may comprise nonneural rim tissue, such as glia and blood vessels[38]. A floor effect will therefore influence the structure-function relationship in advanced glaucoma[33]. A floor effect was not identified in this study, since the study sample consisted of eyes with early to moderate structural damage[10].

The main limitation of our study was its cross-sectional nature. Clinicians should be careful to apply our findings to individual patients longitudinally. Patients may start with a thinner or thicker BMO-MRW, and their individual tipping points may differ from the value we reported. Another limitation was that the average normal BMO-MRW values were calculated from our study cohort. Clinicians should be aware that a normal BMO-MRW value and the percent loss for the tipping point may differ from large population-based data. All of the patients in our study population were Asian, so the structure-function relationship may be different in other ethnic populations.

In conclusion, using "broken-stick" analyses, we identified the tipping point between the BMO-MRW and VF sensitivities in this study. Particularly in early glaucoma, functional loss of vision as measured by standard automated perimetry can be masked until significant structural damage has progressed. We suggest that the tipping point is approximately a 25.9% loss from normal global BMO-MRW values. Therefore, the BMO-MRW measurement may help clinicians to make early decisions regarding a reliable treatment plan before any VF abnormality is detected in the early phases of glaucomatous damage.

## REFERENCES
1 Tham YC, Li X, Wong TY, Quigley HA, Aung T, Cheng CY. Global prevalence of glaucoma and projections of glaucoma burden through 2040: a systematic review and meta-analysis. *Ophthalmology* 2014;121(11):2081-2090.

2 Shah NN, Bowd C, Medeiros FA, Weinreb RN, Sample PA, Hoffmann EM, Zangwill LM. Combining structural and functional testing for detection of glaucoma. *Ophthalmology* 2006;113(9):1593-1602.

3 Nouri-Mahdavi K, Caprioli J. Measuring rates of structural and functional change in glaucoma. *Br J Ophthalmol* 2015;99(7):893-898.

4 Leung CKS, Liu S, Weinreb RN, Lai G, Ye C, Cheung CYL, Pang CP, Tse KK, Lam DSC. Evaluation of retinal nerve fiber layer progression in glaucoma: a prospective analysis with neuroretinal rim and visual field progression. *Ophthalmology* 2011;118(8):1551-1557.

5 Artes PH, Chauhan BC. Longitudinal changes in the visual field and optic disc in glaucoma. *Prog Retin Eye Res* 2005;24(3):333-354.

6 Chauhan BC, Nicolela MT, Artes PH. Incidence and rates of visual field progression after longitudinally measured optic disc change in glaucoma. *Ophthalmology* 2009;116(11):2110-2118.

7 Medeiros FA, Alencar LM, Zangwill LM, Bowd C, Sample PA, Weinreb RN. Prediction of functional loss in glaucoma from progressive optic disc damage. *Arch Ophthalmol* 2009;127(10):1250-1256.

8 Kerrigan-Baumrind LA, Quigley HA, Pease ME, Kerrigan DF, Mitchell RS. Number of ganglion cells in glaucoma eyes compared with threshold visual field tests in the same persons. *Invest Ophthalmol Vis Sci* 2000;41(3):741-748.

9 Wollstein G, Kagemann L, Bilonick RA, Ishikawa H, Folio LS, Gabriele ML, Ungar AK, Duker JS, Fujimoto JG, Schuman JS. Retinal nerve fibre layer and visual function loss in glaucoma: the tipping point. *Br J Ophthalmol* 2012;96(1):47-52.

10 Alasil T, Wang K, Yu F, Field MG, Lee H, Baniasadi N, de Boer JF, Coleman AL, Chen TC. Correlation of retinal nerve fiber layer thickness and visual fields in glaucoma: a broken stick model. *Am J Ophthalmol* 2014;157(5):953-959.

11 Reis ASC, Sharpe GP, Yang H, Nicolela MT, Burgoyne CF, Chauhan BC. Optic disc margin anatomy in patients with glaucoma and normal controls with spectral domain optical coherence tomography. *Ophthalmology* 2012;119(4):738-747.

12 Reis AS, O'Leary N, Yang H, Sharpe GP, Nicolela MT, Burgoyne CF, Chauhan BC. Influence of clinically invisible, but optical coherence tomography detected, optic disc margin anatomy on neuroretinal rim evaluation clinically invisible optic disc margin anatomy. *Invest Ophthalmol Vis Sci* 2012;53(4):1852-1860.

13 Chauhan BC, O'Leary N, AlMobarak FA, Reis AS, Yang H, Sharpe GP, Hutchison DM, Nicolela MT, Burgoyne CF. Enhanced detection of open-angle glaucoma with an anatomically accurate optical coherence tomography-derived neuroretinal rim parameter. *Ophthalmology* 2013;120(3):535-543.

14 Pollet-Villard F, Chiquet C, Romanet JP, Noel C, Aptel F. Structure-function relationships with spectral-domain optical coherence tomography retinal nerve fiber layer and optic nerve head measurements. *Investig Opthalmol Vis Sci* 2014;55(5):2953-2962.

15 Danthurebandara VM, Sharpe GP, Hutchison DM, Denniss J, Nicolela MT, McKendrick AM, Turpin A, Chauhan BC. Enhanced structure-function relationship in glaucoma with an anatomically and geometrically accurate neuroretinal rim measurementstructure-function relationship in glaucoma. *Invest Ophthalmol Vis Sci* 2015;56(1):98-105.

16 Malik R, Belliveau AC, Sharpe GP, Shuba LM, Chauhan BC, Nicolela MT. Diagnostic accuracy of optical coherence tomography and scanning laser tomography for identifying glaucoma in myopic eyes. *Ophthalmology* 2016;123(6):1181-1189.

17 Jonas JB, Budde WM, Panda-Jonas S. Ophthalmoscopic evaluation of the optic nerve head. *Surv Ophthalmol* 1999;43(4):293-320.

18 Garway-Heath DF, Poinoosawmy D, Fitzke FW, Hitchings RA. Mapping the visual field to the optic disc in normal tension glaucoma eyes. *Ophthalmology* 2000;107(10):1809-1815.

19 Hood DC, Kardon RH. A framework for comparing structural and functional measures of glaucomatous damage. *Prog Retin Eye Res* 2007;26(6):688-710.

20 Wu H, de Boer JF, Chen TC. Reproducibility of retinal nerve fiber layer thickness measurements using spectral domain optical coherence tomography. *J Glaucoma* 2011;20(8):470-476.

21 Davies RB. Hypothesis testing when a nuisance parameter is present only under the alternative. *Biometrika* 1987;74(1):33-43.

22 VM M. An R package to fit regression models with broken-line relationships. 2008; Available at: https://cran.r-project.org/web/packages/segmented/segmented.pdf

23 Caprioli J. The importance of rates in glaucoma. *Am J Ophthalmol* 2008;145(2):191-192.

24 Law SK, Kornmann HL, Nilforushan N, Moghimi S, Caprioli J. Evaluation of the "IS" rule to differentiate glaucomatous eyes from normal. *J Glaucoma* 2016;25(1):27-32.

25 Jonas JB, Müller-Bergh JA, Schlötzer-Schrehardt UM, Naumann GO. Histomorphometry of the human optic nerve. *Invest Ophthalmol Vis Sci* 1990;31(4):736-744.

26 Zangwill LM, Weinreb RN, Beiser JA, Berry CC, Cioffi GA, Coleman AL, rick G, Liebmann JM, Brandt JD, Piltz-Seymour JR, Dirkes KA, Vega S, Kass MA, Gordon MO. Baseline topographic optic disc measurements are associated with the development of primary open-angle glaucoma: the confocal scanning laser ophthalmoscopy ancillary study to the ocular hypertension treatment study. *Arch Ophthalmol* 2005;123(9):1188-1197.

27 Zangwill LM, Jain S, Dirkes K, He F, Medeiros FA, Trick GL, Brandt JD, Cioffi GA, Coleman AL, Liebmann JM, Piltz-Seymour JR, Gordon MO, Kass MA, Weinreb RN. The rate of structural change: the confocal scanning laser ophthalmoscopy ancillary study to the ocular hypertension treatment study. *Am J Ophthalmol* 2013;155(6):971-982.

28 Schlottmann PG, De Cilla S, Greenfield DS, Caprioli J, Garway-Heath DF. Relationship between visual field sensitivity and retinal nerve fiber layer thickness as measured by scanning laser polarimetry. *Invest Opthalmol Vis Sci* 2004;45(6):1823-1829.

29 Leung CK, Chong KK, Chan W, Yiu CK, Tso M, Woo J, Tsang MK, Tse KK, Yung WH. Comparative study of retinal nerve fiber layer measurement by StratusOCT and GDx VCC, II: structure/function regression analysis in glaucoma. *Invest Ophthalmol Vis Sci* 2005;46(10):3702-3711.

30 Badlani V, Shahidi M, Shakoor A, Edward DP, Zelkha R, Wilensky J. Nerve fiber layer thickness in glaucoma patients with asymmetric hemifield visual field loss. *J Glaucoma* 2006;15(4):275-280.

31 Yu M, Lin C, Weinreb RN, Lai G, Chiu V, Leung CK. Risk of visual field progression in glaucoma patients with progressive retinal nerve fiber layer thinning: a 5-year prospective study. *Ophthalmology* 2016;123(6):1201-1210.

32 Harwerth RS, Quigley HA. Visual field defects and retinal ganglion cell losses in patients with glaucoma. *Arch Ophthalmol* 2006;124(6):853-859.

33 Lee JW, Kim EA, Otarola F, Morales E, Yu F, Afifi AA, Nouri-Mahdavi K, Caprioli J. The fast component of visual field decay rate correlates with disc rim area change throughout the entire range of glaucomatous damage. *Invest Ophthalmol Vis Sci* 2015;56(10):5997-6006.

34 Shigeeda T, Tomidokoro A, Araie M, Koseki N, Yamamoto S. Long-term follow-up of visual field progression after trabeculectomy in progressive normal-tension glaucoma. *Ophthalmology* 2002;109(4):766-770.

35 Artes PH, O'Leary N, Hutchison DM, Heckler L, Sharpe GP, Nicolela MT, Chauhan BC. Properties of the statpac visual field index. *Invest Ophthalmol Vis Sci* 2011;52(7):4030-4038.

36 Gardiner SK, Johnson CA, Demirel S. The effect of test variability on the structure-function relationship in early glaucoma. *Graefes Arch Clin Exp Ophthalmol* 2012;250(12):1851-1861.

37 Budenz DL, Fredette MJ, Feuer WJ, Anderson DR. Reproducibility of peripapillary retinal nerve fiber thickness measurements with stratus OCT in glaucomatous eyes. *Ophthalmology* 2008;115(4):661-666.

38 Strouthidis NG, Gardiner SK, Sinapis C, Burgoyne CF, Garway-Heath DF. The spatial pattern of neuroretinal rim loss in ocular hypertension. *Invest Ophthalmol Vis Sci* 2009;50(8):3737-3742.